


Damage identification in gravity dams using dynamic coupled hydro-mechanical XFEM

Muyiwa Alalade  · Long Nguyen-Tuan · Frank Wuttke · Tom Lahmer

Received: 29 December 2016 / Accepted: 17 March 2017 / Published online: 4 April 2017
© Springer Science+Business Media Dordrecht 2017

Abstract In order to maximize efficiency and reduce the risk of failure in operational dams, an effective and efficient method which employs the inverse analysis of a dynamic coupled hydro-mechanical problem is proposed. The numerical model is based on the extended finite element model. The proposed method is able to identify cracks which may be detrimental to structural performance and reliability. An attempt is made using both deterministic and heuristic based strategies to solve the ill-posed inverse problem and identify the location, dimension and orientation of the crack. More so, the influence of the search space and conditioning of the cost function in identifying crack parameters are investigated. The proposed method shows promising results in the identification of cracks in a fully operational dam.

Keywords Cracks identification · Inverse modeling · XFEM · Hydro-mechanical coupling · Dynamic loading

1 Introduction

Dams are structures used to retain or control the flow of water in a catchment area, this could be for agricultural purposes (irrigation), flood prevention or for electricity generation. Although the demand for such structures are on the increase to cater for the increasing population and demand for renewable energy, building new dams requires lots of resources, thus the efficiency and operating capacities of existing dams should be maximized.

Today, most dams have been in operation far beyond their designed operation period and as such a decrease in the reliability of such structures is expected. As much as these structures are of great value to communities, a failure in such a structure is in most cases catastrophic, thus great care must be taken in its design, operation and maintenance. In order to assess both the structural integrity and reliability of these structures routine inspections are required. However as a result of the physical sizes and the increasing heterogeneity (with aging) in the material properties of these structures it is often very difficult and tedious to carry out both a qualitative and quantitative assessment of the dams. Thus necessitating the application of numerical methods to simulate the structural behavior and identify regions of weaknesses in the dam. Furthermore, to obtain a more realistic idea of the dams' operation state, it is necessary to consider the effects and interaction of

M. Alalade (✉) · L. Nguyen-Tuan · T. Lahmer
Institute of Structural Mechanics, Bauhaus-Universität,
99423 Weimar, Germany
e-mail: muyiwa.alalade@uni-weimar.de

F. Wuttke
Geomechanics and Geotechnics, Christian-Albrechts-
University, Kiel, Germany

other phenomena on the structure. In this case the hydraulic effect of water seepage into the dam material. This induces pore pressures in addition to the mechanical induced deformation thus generating additional stresses which may impair the safe operation of the dam.

There are a variety of models proposed to analyze the damages or cracks in the dams under dynamic loads. These includes model based on discrete crack approach (Feltrin et al. 1991; Ayari and Saouma 1990; Ahmadi et al. 2001; Ingraffea and Saouma 1985), smeared crack approach (Bhattacharjee and Lger 1994; Lger and Leclerc 1996; Guanglun et al. 2000; Ghaemian and Ghobarah 1999; Lahmer 2010), plastic damage model (Lee and Fenves 1998), discontinuous deformation analysis (DDA) (Jing et al. 2001), mesh-free cracking particles (Rabczuk and Belytschko 2004; Rabczuk et al. 2010), extended finite element methods (XFEM) (Belytschko and Black 1999), and many more. Comparison of cracking process using some of the aforementioned models with application to cracks in dams can be obtained in Pan et al. (2011). The Extended Finite Element Methods (XFEM) is a widely implemented method which is capable of efficiently accounting for cracks, voids and inclusions in the numerical model. Here, nodes of elements containing cracks, voids or inclusions are enriched thus cutting down the additional computational cost required for remeshing (i.e. instead of the calculation and reassembly of all matrix entries, only the enriched nodal values are recalculated) as would be required in standard FEM (Singh et al. 2011). More so, carrying out an inverse analysis require these models to be executed over many iterations (the exact number is influenced by the optimization algorithm selected) thus the XFEM is preferred since only the damaged regions require remeshing.

Recent works in literature on damage modeling using XFEM include works by Zhang et al. (2015) where a dynamic XFEM formulation is applied for crack identification. Furthermore, Zheng et al. (2011) used a cohesive crack model (CCM-based XFEM) to simulate and monitor the cracking process in concrete arch-dams, and Khoei et al. (2014) modeled crack growth in saturated porous media based on an enriched-FEM technique. In Wang et al. (2015), XFEM and incremental dynamic analysis is used to analyze potential failure modes of concrete dams subjected to strong ground motion, noting that as a

result of low tensile resistance of concrete seismic loads cause internal crack damages. An XFEM analysis of seismic crack propagation with upstream and downstream initial cracks was studied by Zhang et al. (2013).

Strategies based on different concepts are available for the calibration and optimization of models in engineering. The aim is to identify model parameters which enables a numerical model to adequately simulate an engineering problem or natural phenomenon. The employed strategies may be deterministic or random. These include the Gradient/Newton methods, which are of the descent methods with line search strategies used in unconstrained nonlinear optimization that gives very fast results when the initial guess is close to the minimum. In Jung et al. (2013) this scheme is implemented in the identification of scatters (cracks, void, inclusions) in heterogeneous elastic material. The Nelder–Mead method is one of the direct search or gradient free strategies for locating the minima of a function. The algorithm was originally published in 1965 and according to Nelder and Mead (1965), it is one of the best known algorithms for multidimensional unconstrained optimization without derivatives. Although strongly dependent on the initial guess, this method has been used to successfully identify cyclic constitutive parameters for unsaturated cyclic macro-element models in Alalade et al. (2016) and model parameters necessary in coupled thermo-hydrromechanical (THM) barrier materials for nuclear waste repositories in Nguyen-Tuan et al. (2009). By re-initializing the Nelder–Mead algorithm using different initial guesses enables the method to act like a global optimizer. The Particle swarm optimization (PSO) is a population based stochastic optimization technique developed by Eberhart and Kennedy (1995), inspired by social behavior of bird flocking or fish schooling. It is a heuristic based global optimizer easily applicable to a number of situations. PSO involves distributing a number of particles in the search space and the objective function of each particle is calculated and the best positions (personal and global) is saved at every iteration. In Nguyen-Tuan et al. (2016), the PSO algorithm was employed in the identification of buffer elements in complex thermo-hydro-mechanical analyses. The genetic algorithm (GA) is also an adaptive global optimizer which draws inspiration from genetics and evolution. Here particles with favorable

traits/solutions are selected, crossed-over (mutated) and evolved to the next generation. This continues till the global optimum is identified. Application of this algorithm in damage identification can be obtained in works by Rabinovich et al. (2007), Rabinovich et al. (2009), Minagawa et al. (2012), Waisman et al. (2010) and Chatzi et al. (2011). The multilevel coordinate search is another optimization strategy used by Nanthakumar et al. (2014) to identify damages in piezoelectric materials. The algorithm converges to the global minima/maxima by balancing both heuristic methods and local methods (Nanthakumar et al. 2016).

Other successful identification of crack/fracture in flat membranes and piezoelectric materials are seen in works of Béchet et al. (2009) and Nguyen-Vinh et al. (2012) where dynamic behavior is considered and in Nanthakumar et al. (2014) where multiple flaws are detected. In Sun et al. (2014) both heuristic and gradient based optimization schemes are applied in a 2-step frame work to identify flaws. Additionally, small scale damages in large structures were identified using a sweeping window in Sun et al. (2015).

A lot has been done with respect to the modeling of damages/cracks and its propagation as a result of both static and dynamic loads on different types of materials, however not much has been done so far with regards to the identification of these damages/cracks in dams considering the hydro-mechanical coupling effects using XFEM under dynamic load. Therefore, in order to practically implement any of the previously discussed damage/fracturing models to dam safety analysis, it is crucial to first and foremost identify probable or existing crack/damage zones before further fracture analysis can be carried out.

This paper aims to efficiently identify cracks in dynamically excited gravity dams using a coupled hydro-mechanical extended finite element model (XFEM). Synthetic measurements taken at different sensitive points on the dam as a result of the dynamic excitation are used in the inverse analysis model to identify the location of the crack in the dam geometry. In the absence of a priori information a 2-step analysis may be required to fine-tune the identified parameters thus increasing the methods' robustness. Both deterministic and random search strategies are employed in the inverse analysis and the results obtained show a promising application of this method to the structural health monitoring of dams.

2 Numerical models

2.1 Coupled hydro-mechanical model

Fluid flow through a porous medium is assumed to be incompressible with constant material densities along the motion of the fluid through varying pressure points in the domain. Material permeability is assumed to be isotropic, with displacement, \mathbf{u} describing the main variable for the mechanical process and pore water pressure, \mathbf{p}_w describing the main variable for the hydraulic process.

The mathematical modeling of the fluid flow structure interaction is described combining the linear momentum balance equation for the mixture solid/water, the general form of the effective stress principle, the constitutive relationship for solid phase relating effective stresses to strains, and the compatibility equation that links strains to displacements. The mass balance equation for water is combined with the general form of Darcys law to describe the flow behavior of the porous medium under the influence of the solid skeleton deformation (Segura and Carol 2008).

The effective stress concept in Eq. 1 explains the characteristics of the effects of fluid saturated fractures on the solid phase. That is, the hydraulic effects of the pore pressures on the normal components of the mechanical stresses. When considering that negative stresses describes the compression state and positive stress the tension state, the effective stress is written differently as would be expected in soil mechanics. A quasi-static stress equilibrium problem is considered for scenarios where the fluid movement in the porous media is slow. Thus the linear momentum balance equation is expressed in Eq. 2, where ρ_a is the density of the porous medium and comprises of both the solid and liquid phase (Zienkiewicz and Shiomi 1984).

$$\sigma' = \sigma + \alpha_b \mathbf{m} \mathbf{p}_w, \quad (1)$$

$$\begin{aligned} \nabla \cdot \sigma - \nabla \mathbf{p}_w + \rho_a \mathbf{g} &= 0 \\ \rho_a &= (1 - n) \rho_s + n \rho_w \end{aligned} \quad (2)$$

where

- σ is the macroscopic total stress tensor (N/m²)
- σ' is the effective stress tensor (N/m²)
- g is the acceleration due to gravity (m/s²)

- ρ_a is the density of porous medium (kg/m^3)
- ρ_s is the density of solids (kg/m^3)
- ρ_w is the density of water (kg/m^3)
- n is the porosity
- \mathbf{p}_w is the water pore pressure vector (N/m^2)
- α_b is the Biot's constant (usually $\alpha = 1$)
- \mathbf{m} is a particular tensor which introduces the influence of fluid pressure in the direction normal to the discontinuity axis ($\mathbf{m} = [1, 1, 1, 0, 0, 0]^T$)

Fluid flow in deformable, saturated porous media is described by the following volume balance equation (Eq. 3) based on mass balance equations of both liquid and solid phases in porous medium.

$$\left(\frac{\alpha_b - n}{\mathbf{K}_s} + \frac{n}{\mathbf{K}_w}\right) \frac{d\mathbf{p}_w}{dt} + \alpha \nabla \cdot \frac{d\mathbf{u}}{dt} + \nabla \cdot \hat{\mathbf{q}} = 0 \quad (3)$$

where

- \mathbf{K}_s and \mathbf{K}_w are the bulk modulus of solid and water (N/m^2),
- \mathbf{u} is the mechanical displacement vector (m).
- $\hat{\mathbf{q}}$ is the fluid flux in (m/s)

When considering a single phase flow with the assumption that the internal fluid friction is less when compared to the friction on the solid-fluid interface and neglecting the turbulence effects, the value of $\hat{\mathbf{q}}$ is assumed to follow Darcy's law in Eq. 4.

$$\hat{\mathbf{q}} = -\frac{\kappa}{\mu_w} (\nabla p_w - \rho_w \mathbf{g}), \quad (4)$$

where

- κ is the intrinsic permeability (m^2)
- μ_w is the fluid dynamic viscosity (Ns/m^2)

Applying standard FEM procedures found in literature on fluid flow in porous media (Zienkiewicz and Shiomi 1984; Zienkiewicz et al. 1990; Coussy 1995; Lewis and Schrefler 1998; Khoei 2014), the coupled hydro-mechanical behavior of a porous material is expressed thus:

$$\int_{\Omega} \mathbf{B}_u^T \sigma' d\Omega - \mathbf{Q} \mathbf{p}_w = \mathbf{f}_{(t)} \quad (5)$$

$$\mathbf{S} \frac{d\mathbf{p}_w}{dt} + \mathbf{H} \mathbf{p}_w + \mathbf{Q} \frac{d\mathbf{u}}{dt} = \mathbf{q}_{(t)} \quad (6)$$

where

The coupling matrix, $\mathbf{Q} = \int_{\Omega} \mathbf{B}_u^T \alpha \mathbf{m} \mathbf{N}_p d\Omega \quad (7)$

The permeability matrix, $\mathbf{H} = \int_{\Omega} (\nabla \mathbf{N}_p)^T \kappa \nabla \mathbf{N}_p d\Omega \quad (8)$

The compressibility matrix,

$$\mathbf{S} = \int_{\Omega} \mathbf{N}_p^T \left(\frac{\alpha - n}{\mathbf{K}_s} + \frac{n}{\mathbf{K}_w}\right) \mathbf{N}_p d\Omega \quad (9)$$

The fluid flux vector, $\mathbf{q} = \int_{\Gamma} \nabla \mathbf{N}_p^T \hat{\mathbf{q}} d\Gamma \quad (10)$

However, from the constitutive law for stress-strain behavior, $\sigma' = \mathbf{D}\epsilon$ and $\epsilon = \mathbf{B}_u \mathbf{u}$, σ' can be substituted in Eq. 5. Thus the first term in (5) can be expressed as the traditional stiffness matrix, $\mathbf{K} = \int_{\Omega} \mathbf{B}_u^T \mathbf{D} \mathbf{B}_u d\Omega$ as obtained in Eq. 11. To consider the effect of a time varying force $\mathbf{f}_{(t)}$ on the analysis, (11) is extended considering the inertia term and in line with Newtons law of motion leading to the expression in Eq. 12. An explicit derivation of 12 is found in Zienkiewicz and Shiomi (1984).

$$\mathbf{K} \mathbf{u} - \mathbf{Q} \mathbf{p}_w = \mathbf{f}_{(t)} \quad (11)$$

$$\mathbf{M} \ddot{\mathbf{u}} + \mathbf{C} \dot{\mathbf{u}} + \mathbf{K} \mathbf{u} - \mathbf{Q} \mathbf{p}_w = \mathbf{f}_{(t)} \quad (12)$$

$$\mathbf{M} = \int_{\Omega} \mathbf{N}_u^T \rho \mathbf{N}_u d\Omega^e, \quad (13)$$

$$\mathbf{f} = \int_{\Omega} \mathbf{N}_u^T \rho_a \mathbf{b} d\Omega + \int_{\Gamma_t} \mathbf{N}_u^T \bar{\mathbf{t}} d\Gamma \quad (14)$$

where

- \mathbf{M} is the mass matrix
- \mathbf{C} is the damping matrix expressed in Eq. 15
- \mathbf{N}_u is the displacement shape function
- \mathbf{N}_p is the pressure shape function
- \mathbf{B} is a matrix containing the derivatives of the shape function
- \mathbf{D} is a stress/strain matrix which is a function of the materials Youngs' modulus, E and Poisson's ratio, ν
- \mathbf{f} is the external force vector
- \mathbf{b} is the vector of body force
- $\ddot{\mathbf{u}}$ and $\dot{\mathbf{u}}$ are the acceleration and velocity vector
- $\bar{\mathbf{t}}$ is the surface traction vector

$$\mathbf{C} = \alpha \mathbf{M} + \beta \mathbf{K}. \tag{15}$$

The α and β coefficients in Eq. 15 are the Rayleigh damping coefficients. These can be obtained from experiments or through other methods proposed in literature. The method proposed by Chowdhury and Dasgupta (2003) was used to calculate α and β with a damping ratio of 2and5% considering the first 3 modes. The Newmark scheme Chopra (1995) is applied in solving the dynamic mechanical system such that the values of the nodal displacements, velocities and accelerations are obtained. Depending on the β^* and γ^* values used to implement the scheme, it is necessary that the time step δt chosen is less than the critical time step T_c to ensure stability. The resulting displacements obtained are used to compute the strains and stresses as done in standard FEM calculations. The hydraulic effect of water seepage into the dam material causes an increase in the pore pressures and in addition to the mechanical induced deformation this generates additional stresses in the dam.

$$\begin{aligned} & \begin{bmatrix} \mathbf{M} & 0 \\ 0 & 0 \end{bmatrix} \begin{Bmatrix} \ddot{\mathbf{u}}(t) \\ \ddot{\mathbf{p}}(t) \end{Bmatrix} + \begin{bmatrix} \mathbf{C} & 0 \\ \mathbf{Q}^T & \mathbf{S} \end{bmatrix} \begin{Bmatrix} \dot{\mathbf{u}}(t) \\ \dot{\mathbf{p}}(t) \end{Bmatrix} \\ & + \begin{bmatrix} \mathbf{K} & -\mathbf{Q} \\ 0 & \mathbf{H} \end{bmatrix} \begin{Bmatrix} \mathbf{u}(t) \\ \mathbf{p}(t) \end{Bmatrix} \\ & = \begin{Bmatrix} \mathbf{f}(t) \\ \mathbf{q}(t) \end{Bmatrix} \end{aligned} \tag{16}$$

The coupled dynamic hydro-mechanical model expressed in Eq. 16 can be solved simultaneously (monolithic) for the resulting displacements and pore water pressures or in a staggered procedure. In the staggered procedure each equation is solved (probably using different solvers) at each time step and the solution of one parameter is used to ‘drive’ the solution for the other parameter at the next time step.

2.2 Dam crack modeling

The extended finite element method (XFEM) introduced by Belytschko and Black (1999) is capable of incorporating the local enrichment into the approximation space within the framework of finite elements. The enriched approximation of the extended finite element method for the displacement field u can be

written according to Belytschko et al. (2009) in Eq. 17.

$$\begin{aligned} \mathbf{u}(x, t) \approx \mathbf{u}^h(x, t) &= \sum_{I \in \mathbb{N}} \mathbf{N}_{uI}(x) \bar{u}_I(t) \\ &+ \sum_{J \in \mathbb{N}^{dis}} \mathbf{N}_{uJ}(x) (H(\varphi(x)) - H(\varphi(x_J))), \bar{\mathbf{a}}_J(t) \\ &+ \sum_{G \in \mathbb{N}^{tip}} \mathbf{N}_{uG}(x) \sum_{\alpha=1}^4 (\beta_{\alpha}(x) - \beta_{\alpha}(x_G)), \bar{\mathbf{b}}_{\alpha G}(t) \end{aligned} \tag{17}$$

where

- \mathbb{N} is the set of all nodal points
- \mathbb{N}^{dis} is the set of enriched nodes whose support is bisected by the crack
- \mathbb{N}^{tip} is the set of nodes which contain the crack-tip in the support of their shape functions enriched by the asymptotic functions
- $\bar{u}_I(t)$ are the unknown standard nodal displacements at I th node
- $\bar{a}_J(t)$ are the unknown enriched nodal degrees of freedom associated with the Heaviside at node J enrichment function at node J
- $\bar{b}_{\alpha G}(t)$ are the additional enriched nodal degrees of freedom associated with the asymptotic functions at node G
- $\mathbf{N}_u(x)$ are the standard displacement shape functions
- $H(\varphi(x))$ is the Heaviside jump function used to model the discontinuity due to different displacement fields on either sides of the crack
- $\beta_{\alpha}(x)$ are the asymptotic functions extracted from the analytic solution and used to model the displacement field at the crack-tip region

$H(\varphi(x))$ is defined in Eq. 18 and $\beta_{\alpha}(x)$ in Eq. 19

$$H(\varphi(x)) = \begin{cases} +1 & \varphi(x) \geq 0 \\ 0 & \varphi(x) < x \end{cases} \tag{18}$$

$$\begin{aligned} \beta(r, \theta) &= \{\beta_1, \beta_2, \beta_3, \beta_4\} \\ &= \left\{ \sqrt{r} \sin \frac{\theta}{2}, \sqrt{r} \cos \frac{\theta}{2}, \sqrt{r} \sin \frac{\theta}{2} \sin \theta, \sqrt{r} \cos \frac{\theta}{2} \sin \theta \right\} \end{aligned} \tag{19}$$

The signed distance function $\varphi(x)$ in Eq. 18 is defined based on the absolute value of level set function as $\varphi(x) = \min \|x - x^*\| \text{sign}((x - x^*) \cdot \mathbf{n}_{\Gamma_d})$.

Where x^* is a point on the discontinuity, which has the closest distance from the point x and n_{Γ_d} . The interchangeability of the Heaviside function and the sign of the level-set function though common in literature, leads to similar results (Borst et al. 2006).

The approximation of the pressure field in XFEM is dependent on the type of discontinuity being considered. In cases where a void is encountered, the discontinuity is weak because the domain does not impose any discontinuity in the fluid flow thus standard FEM shape functions without any enrichment are adequate for the approximation. However, cracks introduce strong discontinuities in the fluid flow hence the standard shape functions and also Heaviside enrichment are required to approximate the pore pressure. Thus the enriched approximation of the pressure field p can be expressed according to R  thor   et al. (2007) in Eq. 20.

$$\mathbf{p}(x, t) \approx \mathbf{p}^h(x, t) = \sum_{I \in \mathbb{N}} \mathbf{N}_{pI}(x) \bar{p}_I(t) + \sum_{J \in \mathbb{N}^{dis}} \mathbf{N}_{pJ}(x) (\psi(x) - \psi(x_J)) \bar{c}_J(t) \tag{20}$$

where

- $\bar{p}_I(t)$ is the unknown nodal pressure at the I th node
- $\bar{c}_J(t)$ is the unknown enriched nodal degree of freedom associated with the level-set function at node J
- $\mathbf{N}_{pI}(x)$ are the standard pressure shape functions
- $\psi(x)$ is the modified level set function given as

$$\psi(x) = \sum_{I \in \mathbb{N}^{dis}} \mathbf{N}_{pI}(x) |\varphi_I| - \left| \sum_{I \in \mathbb{N}^{dis}} \mathbf{N}_{pI}(x) \varphi_I \right|. \tag{21}$$

The level set functions are applied in the enriched shape functions to enable numerical computation involving curved objects and surfaces on a fixed grid without having to parameterize the objects (Osher and Sethian 1988). In order to take into consideration the discontinuity in the fluid pressure gradient on elements the relation in (21) is applied. It has a ridge centered on the interpolated interface and vanishes in elements not containing the material interface. This results in the enrichment function being zero in the blending elements and the unwanted terms appearing in the approximating space of the blending elements are avoided. Thus,

the enrichment function is continuous across the fracture, while its gradient is discontinuous in the normal direction to the discontinuity. Possessing this desirable property, the enrichment function enables the approximate pressure field to be discontinuous in its normal derivative across the discontinuity, accounting for the leak-off of the fluid from the discontinuity (Khoei 2014). A detailed description of the implementation of this enrichment technique is obtainable in Zlotnik et al. (2007).

Considering the necessary shape function enrichment as a result of voids and cracks in the structure, each constituent of the coupled hydro-mechanical matrix in (16) is extended to include both the crack tip and Heaviside enrichment as obtained in Eq. 22 for the mechanical part considering damping, and (23) for the pore water pressure part. These enrichment are implemented for elements that contain crack tips and also for elements completely cut through by a crack. In situations where nodes belong to a set of elements enriched with the crack-tip asymptotic function and Heaviside enriched element, the crack tip enrichment is used.

$$\begin{aligned} & \begin{bmatrix} \mathbf{M}_{uu} & \mathbf{M}_{ua} & \mathbf{M}_{ub} \\ \mathbf{M}_{au} & \mathbf{M}_{aa} & \mathbf{M}_{ab} \\ \mathbf{M}_{bu} & \mathbf{M}_{ba} & \mathbf{M}_{bb} \end{bmatrix} \begin{Bmatrix} \ddot{\mathbf{u}} \\ \dot{\bar{\mathbf{a}}} \\ \dot{\bar{\mathbf{b}}} \end{Bmatrix} + \begin{bmatrix} \mathbf{C}_{uu} & \mathbf{C}_{ua} & \mathbf{C}_{ub} \\ \mathbf{C}_{au} & \mathbf{C}_{aa} & \mathbf{C}_{ab} \\ \mathbf{C}_{bu} & \mathbf{K}_{ba} & \mathbf{C}_{bb} \end{bmatrix} \begin{Bmatrix} \dot{\mathbf{u}} \\ \dot{\bar{\mathbf{a}}} \\ \dot{\bar{\mathbf{b}}} \end{Bmatrix} \\ & + \begin{bmatrix} \mathbf{K}_{uu} & \mathbf{K}_{ua} & \mathbf{K}_{ub} \\ \mathbf{K}_{au} & \mathbf{K}_{aa} & \mathbf{K}_{ab} \\ \mathbf{K}_{bu} & \mathbf{K}_{ba} & \mathbf{K}_{bb} \end{bmatrix} \begin{Bmatrix} \mathbf{u} \\ \bar{\mathbf{a}} \\ \bar{\mathbf{b}} \end{Bmatrix} \\ & = \begin{Bmatrix} \mathbf{f}_u \\ \mathbf{f}_a \\ \mathbf{f}_b \end{Bmatrix} + \begin{bmatrix} \mathbf{Q}_{up} & \mathbf{Q}_{uc} \\ \mathbf{Q}_{ap} & \mathbf{Q}_{ac} \\ \mathbf{Q}_{bp} & \mathbf{Q}_{bc} \end{bmatrix} \begin{Bmatrix} \bar{\mathbf{p}} \\ \bar{\mathbf{c}} \end{Bmatrix}, \tag{22} \end{aligned}$$

$$\begin{aligned} & \begin{bmatrix} \mathbf{S}_{pp} & \mathbf{S}_{pc} \\ \mathbf{S}_{cp} & \mathbf{S}_{cc} \end{bmatrix} \begin{Bmatrix} \dot{\bar{\mathbf{p}}} \\ \dot{\bar{\mathbf{c}}} \end{Bmatrix} + \begin{bmatrix} \mathbf{H}_{pp} & \mathbf{H}_{pc} \\ \mathbf{H}_{cp} & \mathbf{H}_{cc} \end{bmatrix} \begin{Bmatrix} \bar{\mathbf{p}} \\ \bar{\mathbf{c}} \end{Bmatrix} = \begin{Bmatrix} \mathbf{q}_p \\ \mathbf{q}_c \end{Bmatrix} \\ & - \begin{bmatrix} \mathbf{Q}_{up}^T & \mathbf{Q}_{ap}^T & \mathbf{Q}_{bp}^T \\ \mathbf{Q}_{uc}^T & \mathbf{Q}_{ac}^T & \mathbf{Q}_{bc}^T \end{bmatrix} \begin{Bmatrix} \dot{\mathbf{u}} \\ \dot{\bar{\mathbf{a}}} \\ \dot{\bar{\mathbf{b}}} \end{Bmatrix} \tag{23} \end{aligned}$$

The XFEM mass matrix \mathbb{M} , stiffness matrix \mathbb{K} , coupling matrix \mathbb{Q} , compressibility matrix \mathbb{S} , permeability matrix \mathbb{H} and force \mathbf{f} and fluid flux \mathbf{q} vectors are defined in (24)–(30) respectively.

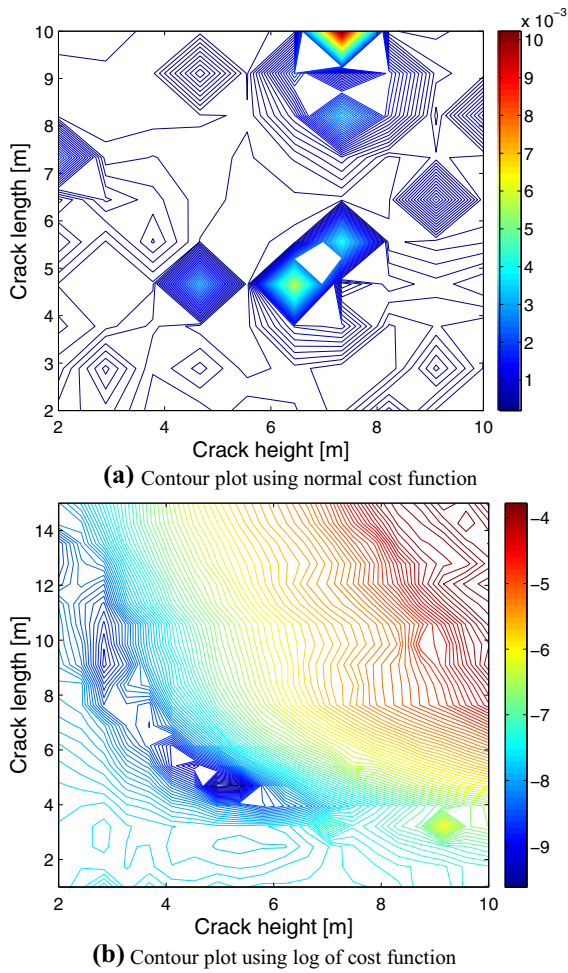


Fig. 1 Effect of cost function definition on the identification of the global minima. In (a) the contour plot is very flat with many minimum points, however using the log of the cost function in (b) accentuates the cost function values thus increasing the probability of converging to the global minima

Table 1 Dam properties

H (m)	B (m)	L (m)	E (MPa)	ν	ρ (kg/m ³)
28	19	0.1	24×10^3	0.15	24×10^2
α	β	β^*	γ^*	δt	T (s)
-0.354	0.0162	0.5	0.25	0.1	4

$$\mathbb{M}_{\vartheta\varpi} = \int_{\Omega} (\mathbf{N}_u^{\vartheta})^T \rho_a \mathbf{N}_u^{\varpi} d\Omega \quad (24)$$

Table 2 Hydro-mechanical dam properties

ρ_w (kg/m ³)	K_w (N/m ²)	n
1000	2.2×10^6	1×10^{-6}
n	μ (N/s ²)	κ (m ²)
1×10^{-3}	1×10^{-18}	1.12×10^{-12}

$$\mathbb{K}_{\vartheta\varpi} = \int_{\Omega} (\mathbf{B}_u^{\vartheta})^T \mathbf{D} \mathbf{B}_u^{\varpi} d\Omega \quad (25)$$

$$\mathbb{Q}_{\vartheta\varpi} = \int_{\Omega} (\mathbf{B}_u^{\vartheta})^T \alpha \mathbf{m} \mathbf{N}_u^{\varpi} d\Omega \quad (26)$$

$$\mathbf{f}_{\alpha} = \int_{\Omega} (\mathbf{N}_u^{\alpha})^T \rho_a \mathbf{b} d\Omega + \int_{\Gamma_i} (\mathbf{N}_u^{\alpha})^T \bar{\mathbf{t}} d\Gamma \quad (27)$$

$$\mathbb{S}_{\delta\gamma} = \int_{\Omega} (\mathbf{N}_p^{\delta})^T \left(\frac{\alpha - n}{\mathbf{K}_s} + \frac{n}{\mathbf{K}_w} \right) \mathbf{N}_p^{\gamma} d\Omega \quad (28)$$

$$\mathbb{H}_{\delta\gamma} = \int_{\Omega} (\nabla \mathbf{N}_p^{\delta})^T \kappa \nabla \mathbf{N}_p^{\gamma} d\Omega \quad (29)$$

$$\mathbf{q}_{\delta} = \int_{\Omega} (\mathbf{N}_p^{\delta})^T \kappa \cdot \rho_w \mathbf{b} d\Omega - \int_{\Gamma_w} (\mathbf{N}_p^{\delta})^T \hat{\mathbf{q}} d\Gamma \quad (30)$$

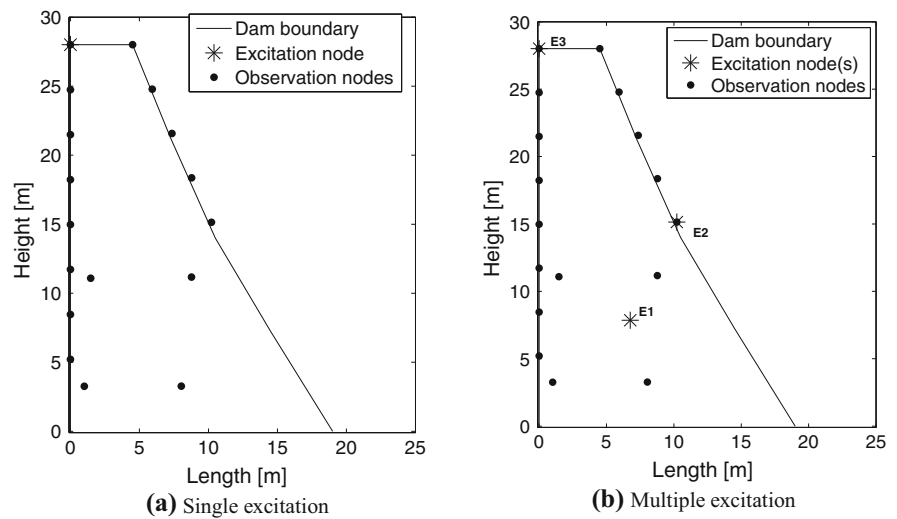
where ϑ and ϖ denote standard and enriched (i.e. Heaviside or asymptotic-tip) displacements functions, whereas δ and γ denote standard and enriched pressure functions. Detailed information on the integration of (24)–(30) for each term in the matrix of (22) and (23) are obtained in Zhang et al. (2015) and Nanthakumar et al. (2014). To take into account discontinuity on the enriched elements during numerical integration, polar integration approach proposed in Chahine et al. (2007) is applied for these enhanced shape functions.

The coupled hydro-mechanical XFEM model can be solved in the time and frequency domain, thus generating the dam response as a function of time as given in (31) or frequency as in (32).

$$\begin{aligned} \mathbb{S}\dot{\mathbf{p}} + \mathbb{H}\mathbf{p} + \mathbb{Q}^T \dot{\mathbf{u}} &= \mathbf{q} \\ \mathbb{M}\ddot{\mathbf{u}} + \mathbb{C}\dot{\mathbf{u}} + \mathbb{K}\mathbf{u} - \mathbb{Q}\mathbf{p} &= \mathbf{f} \end{aligned} \quad (31)$$

$$\begin{aligned} \mathbf{p}_{(\omega)} &= (i\omega\mathbb{S} + \mathbb{H})^{-1} \mathbf{q}_{(\omega)} \\ \mathbf{u}_{(\omega)} &= (-\omega^2\mathbb{M} + i\omega\mathbb{C} + \mathbb{K})^{-1} \mathbf{f}_{(\omega)} + \mathbb{Q}\mathbf{p}_{(\omega)} \end{aligned} \quad (32)$$

Fig. 2 Dam excitation and observation points. **a** The acquisition set-up with a single excitation point and **b** the location of multiple excitation points



In this work a staggered procedure incorporating the Newmark time integration scheme and the forward finite difference method is used to solve the mechanical and pore pressure part of the coupled hydro-mechanical equation.

3 Inverse analysis

The objective of the inverse analysis is to obtain reliable model input values by minimizing the error between experimental data (describing in most cases a phenomena) and numerical results obtained from a mathematical model developed to simulate (as close as possible) the natural phenomena. With the solution obtained from the inverse analysis, it is possible to ascertain and monitor the ‘health’ (state) of the structure or also to simulate the response of the structure during extreme conditions. The parameters obtained can also give an idea of the location of heterogeneity and damages.

If the location of the crack is well parameterized a priori, local and global search methods in the context of non-linear optimization can be applied. One of such global strategies is the particle swarm optimization (PSO) developed by Eberhart and Kennedy (1995) and inspired by social behavior of bird flocking or fish schooling. It is a heuristic based global optimizer easily applicable to a number of situations. It consists of generating random particles in the search space, and at each time step, changing the velocity of

(accelerating) each particle toward its personal best, P_{best} and local best, L_{best} locations. Acceleration is weighted by a random term, with separate random numbers being generated for acceleration toward P_{best} and L_{best} locations. Particle velocity is calculated in Eq. 33 and the updated particle position is calculated from Eq. 34.

$$v = v_{cur} + c_1 \Psi(P_{best} - P_{cur}) + c_2 \Psi(G_{best} - P_{cur}) \quad (33)$$

where Ψ contains random numbers between 0 and 1, and c_1 and c_2 are learning factors.

$$P_{new} = P_{cur} + v_{cur} \quad (34)$$

Other options include the use of local optimizer such the Nelder–Mead method, which is one of the direct search or gradient free strategies for locating the minima of a function. According to Nelder and Mead (1965), it is one of the best known algorithms for multidimensional unconstrained optimization without derivatives.

The objective function being minimized (Eq. 35) is the sum of squared error between the dam response recorded by the sensors and the numerical response generated by the coupled hydro-mechanical XFEM. The response may either be in the frequency or time domain. Quiet a number of methods for the error minimization exists in literature (such as the previously mentioned algorithms). However, to efficiently obtain reliable solutions a deep understanding of the model behavior is required in order to select an

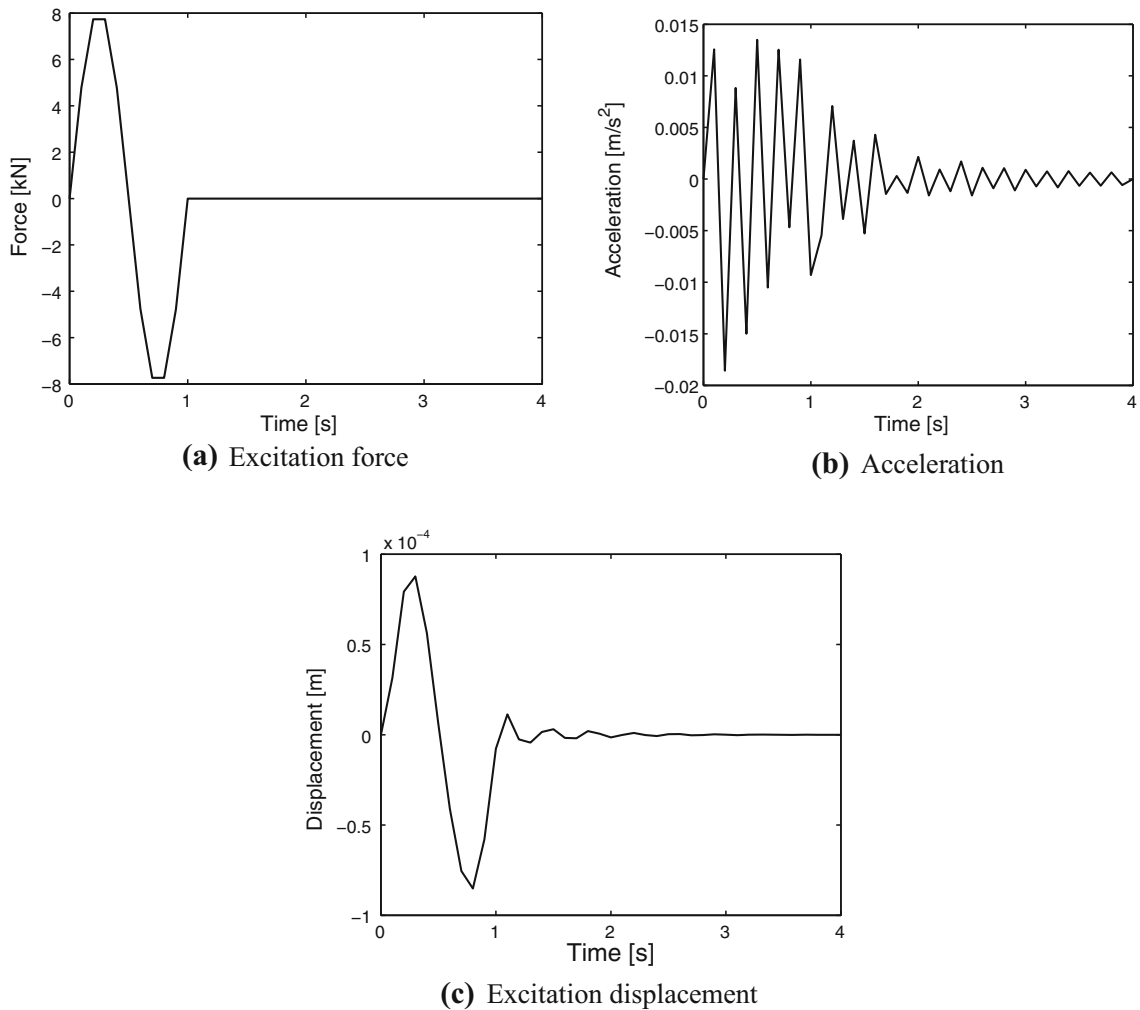


Fig. 3 Dynamic load on dam showing (a) the force time history, (b) the resulting acceleration and (c) displacement due to the dynamic excitation

appropriate method. In the case where the problem is ill-posed (which is generally encountered in engineering), convexification of the objective function is necessary by the use of a regularization strategy as applied in Alalade et al. (2015) if a deterministic optimization method is employed.

$$C_f(p) = \sum_i^n \sum_j^s (\ddot{\mathbf{U}}_{(j,t_i,p)}^{mod} - \ddot{\mathbf{U}}_{(j,t_i)}^{exp})^2 + \kappa \mathcal{R}(j_i, t_i, \mathbf{p}_m) \tag{35}$$

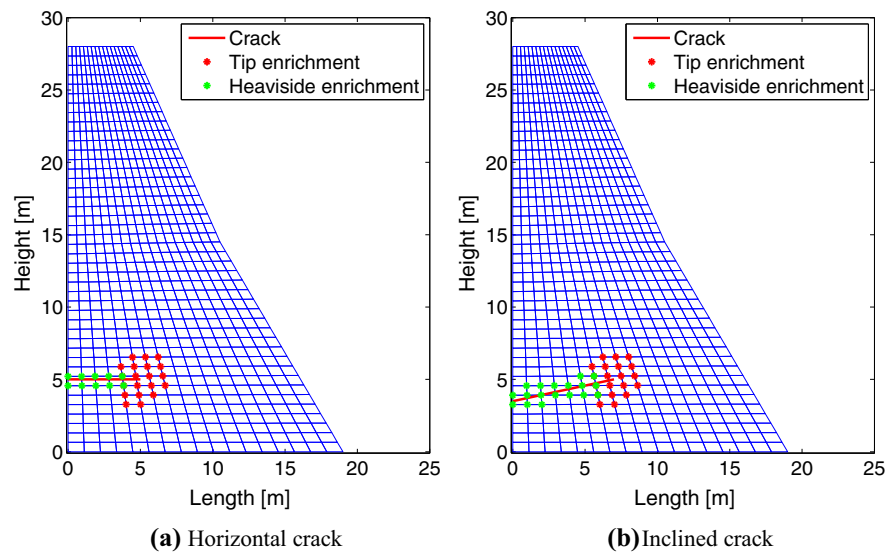
where

- C_f is the cost function to be minimized.
 $C_f : \mathbb{R}^n \times \mathbb{R}^s \rightarrow \mathbb{R}$

- $\ddot{\mathbf{U}}_{(j,t_i,p)}^{mod}$ is the dam response recorded during the numerical simulation at each sensor
- $\ddot{\mathbf{U}}_{(j,t_i)}^{exp}$ is the dam response recorded at each sensor on the dam site (e.g. accelerometer)
- \mathbf{p}_m is a vector of $\mathbb{M}, \mathbb{K}, \mathbb{C}, \mathbb{Q}, \text{HandS}, p \in \mathbb{R}^{\tilde{c}}$
- \tilde{c} is the number of crack descriptors
- \mathcal{R} is regularizing term and $\kappa > 0$
- t_i is the time step at each point
- s is the total number of sensors
- n is the total number of data points

To further improve the chances of identifying the global minima, certain constraints imposed on the analysis include:

Fig. 4 Dam geometry and mesh (damaged XFEM) showing the location and orientation of the crack



1. Reduction of the search space since cracks are assumed to be common and more critical in the lower 5m of the dam. This region is considered critical due to the fact that higher pressures are expected, abrasion from sediments may be pronounced and also difficult to visually inspect. In addition, the dam is equipped with an inspection/drainage canal through which damages above 5m can be noticed by the amount of water seeping into the canal from above.
2. Using the log of the cost function for the parameter search. It should be noted here that negative values in the contour plot results from the log of values less than 1 being negative.
3. Using multiple excitation points instead of a single point for the analysis. This is done by carrying out the excitation at various points sequentially thus leading to the new cost function in Eq. 36 which is a function of all the excitation points. Where m is the number of excitation sources and $C_f(p)$ has been defined in Eq. 35

$$C_f(m) = \sum_i^m C_f(p)_i \quad (36)$$

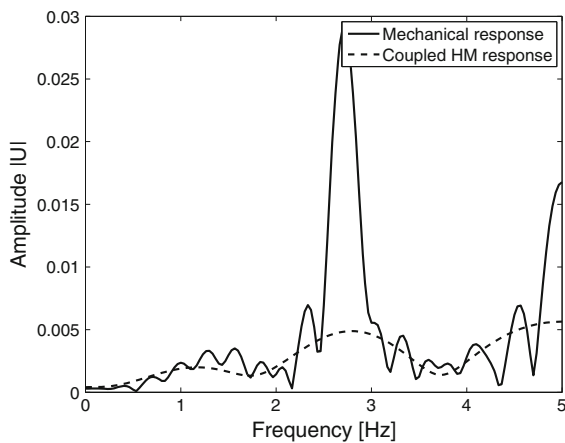
The effect of these constraints can first be seen in the contour plots of Fig. 1. These plots show points of local and global minima with respect to the crack parameters. It can be seen from the comparison that using the log of the cost function makes some of the

local minima less pronounced. This makes the contour plot smoother and increases the chances of convergence to a global minima.

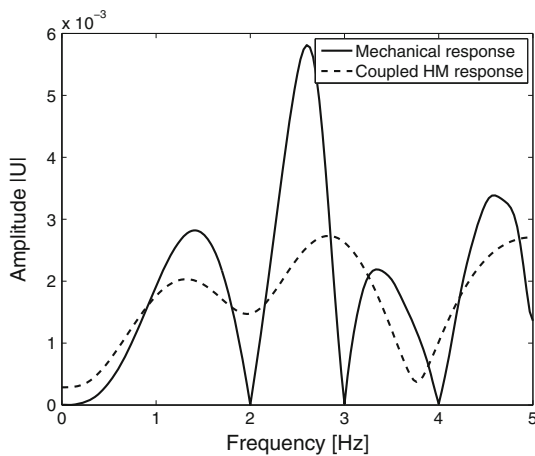
4 Numerical simulation

4.1 Forward model

A masonry gravity dam (similar to the Fuewigge dam) with mechanical and hydraulic properties in Tables 1 and 2 is used for the numerical simulation. Plane stress problem is considered here and the dam thickness, L is taken as 0.1m. In order to validate the numerical model and to investigate the influence of the hydraulic coupling on the dam structure, the dam is dynamically excited at the top of the upstream face in Fig. 2a and at multiple points in Fig. 2b and the response at selected points (sensor location) are recorded. The input force amplitude is obtained from the hydrostatic force acting at the node on the top of the dam upstream face. The force and its resulting acceleration and displacement time histories are obtained in Fig. 3. This excitation is applied for both the mechanical case and also the coupled hydro-mechanical case i.e. without and with the influence of pore water pressure on the displacements. To obtain the generated stresses and strains induced on a dynamically excited dam considering the hydraulic coupled effect on the dam response (i.e. solving the coupled HM problem in Eqs. 22 and (23)) and two different cracks patterns (horizontal and



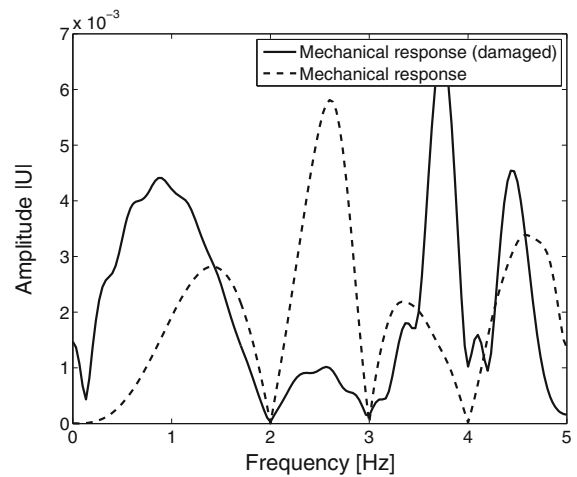
(a) Frequency response for undamped case



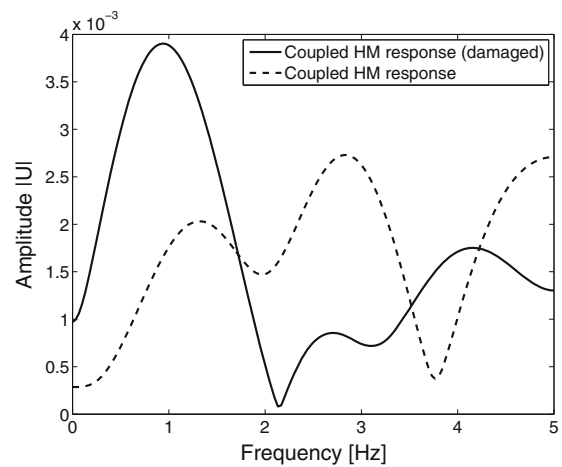
(b) Frequency response for damped case

Fig. 5 Comparison between coupled and uncoupled frequency response at excitation node. **a, b** The amplitude reduction due to the consideration of hydraulic effects on the dam material. In **(a)** structural damping is not considered thus the higher amplitude response

inclined) with coordinates (0, 5), (5, 5) and (0, 3.5), (7, 5) as obtained in Fig. 4, it is necessary to solve the coupled hydro-mechanical equation derived in Eq. 16. There exists several ways of solving this equation, here it is solved by splitting the matrix into two equations as obtained in Eq. 31. First the pore pressures are obtained using the forward difference method, then the mechanical equation is updated with the values of \mathbf{p} and solved using the Newmark time integration scheme to obtain the coupled hydro-mechanical displacements. Results obtained in Fig. 5 show the damping effect of water on the dynamic



(a) Mechanical response



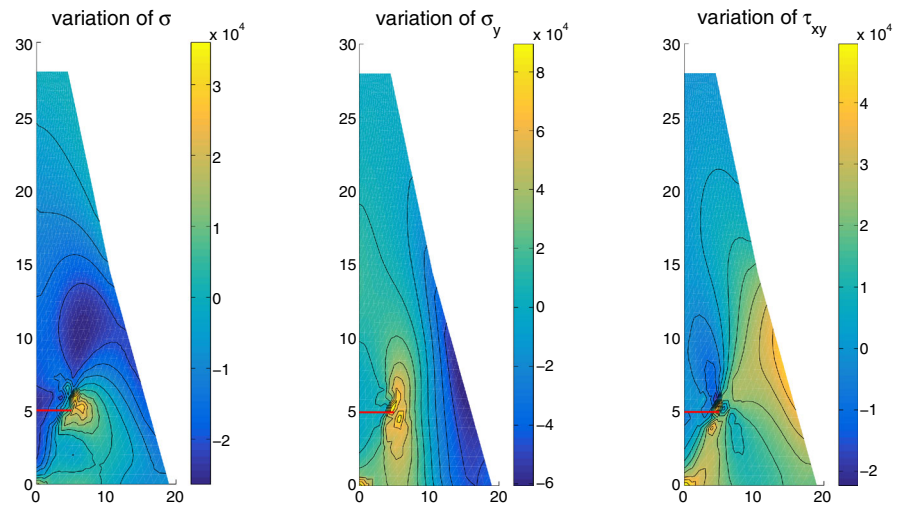
(b) Coupled hydro-mechanical response

Fig. 6 Comparison between damaged and undamaged frequency response at excitation node. With or without the consideration of hydraulic coupling, the model simulates the reduction in the fundamental frequency due to damage in **(a, b)**

behavior of the dam (undamaged) both with and without the consideration of structural damping.

Furthermore, as a result of stiffness degradation due to damages/crack in the structure, an increase in the response amplitude and also a corresponding reduction in fundamental frequency of the dam would be expected. This can be observed in Fig. 6 where a comparison is made between the response of the dam when damaged (i.e. XFEM simulation) and also undamaged (i.e. homogeneous material FEM simulation) for both the mechanical and coupled cases. The stresses induced on the dam due to the dynamic loads

Fig. 7 Stress profile [in (Pa)] at max. recorded displacement [0.9 (s)]



at point $E1$ in Fig. 2b and the presence of a horizontal crack is obtained in Fig. 7.

4.2 Crack identification

In practice the acquisition of the needed data is done via acceleration sensors (Geo-phones) or other types of sensors instrumented on the dam to record various types of vibrations which after undergoing processing is used for the inverse modeling. However in this case, the data used for the damage identification is numerically generated i.e. for a known crack location responses of sensor nodes from the implementation of the forward problem is used. This has the advantage of providing more information on the applied optimization strategy and also sensitivities of parameters related to both the forward and inverse model. The setup is made up of 17 sensors, 13 of the sensors are distributed on the dam upstream and downstream face while 4 are installed within the dam structure itself. Installation is done by drilling into to structure from the inspection tunnel. In the event where difficulty exist in sensor installation on the dam upstream, the proposed acquisition set-up can be adapted to the prevailing site conditions.

Before carrying out the inverse analysis, it is necessary to come up with an effective arrangement of sensors and also select measurements that capture change in structural behavior due to damage. This was achieved by changing the damage location and comparing the average response recorded by each sensor on dam for different crack locations both in the

frequency and time domain. From the results obtained in Fig. 8, it can be observed that the frequency domain (as compared to the time domain) shows more sensitivity to the change in crack location on the dam response. A clearer picture can be seen by comparing Figs. 9 with 10. The contour and surface plots for a time domain analysis in Fig. 9 contains trough-like regions of both local and global minima thus leading to non-unique values. However, when a frequency domain analysis is employed as seen in Fig. 10, the trough-like features are almost absent and a global minima is clearly defined. The frequency domain response is more sensitive to crack location, thus it is preferred for carrying out the inverse analysis. More information on frequency domain inverse analysis for poroelastic material can be obtained in Lahmer and Rafajłowicz (2017).

The parameters used for identifying the crack are the coordinates of the crack tips ($[x_1 \ y_1; x_2 \ y_2]$). Cracks that originate from the dam face are considered more critical, thus $x_1 = 0$ and both horizontal cracks ($y_1 = y_2$) and inclined cracks ($y_1 \neq y_2$) are assumed. A parameter dependency analysis is carried out using contour and surface plots. Results obtained in Figs. 9 and 10 show that the model is ill-posed and depending on the search strategy employed convexification would be required to improve the chances of convergence. In addition to this, a lower 'degree of ill-posedness' (i.e. number of non-unique values) was observed from the contour plot in the frequency domain as compared to the time domain, thus favoring a frequency based inverse analysis.

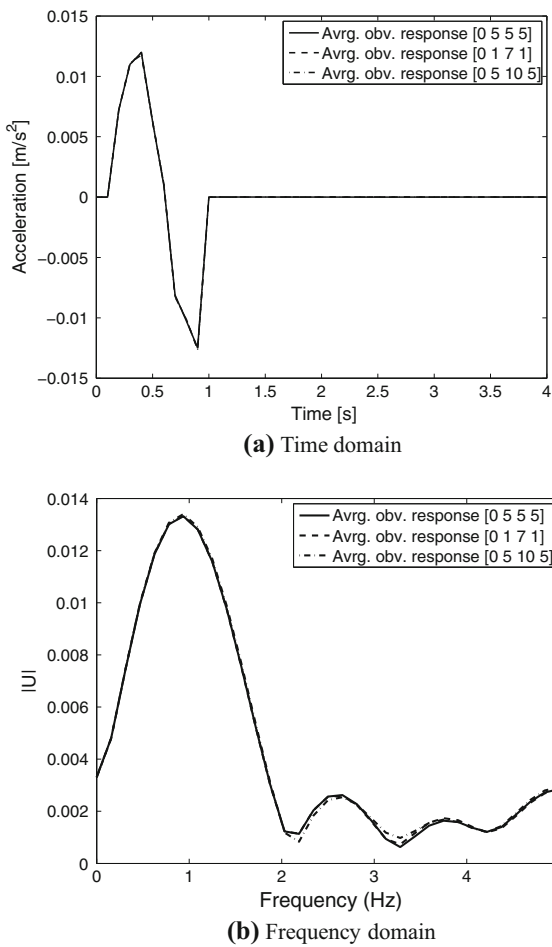


Fig. 8 Response comparison for different crack location. In (a) the time domain response shows very little sensitivity to crack location. However in (b) notable change in frequency response of the dam for different crack location can be observed thus making it slightly convenient to use

An attempt was made to use the constrained and unconstrained Nelder-Mead algorithm to locate the global minima, however irrespective of the application of aforementioned methods the algorithm did not converge to the expected values. The particle swarm optimization PSO on the other hand was able to produce better results. From our observations of the model parameter dependencies in Figs. 10 and 11, random search strategies such as PSO seem to be a better suited method. More so, it can be run using ‘parallel-computing’ thus decreasing computational costs. The algorithm was run using 24 particles (i.e. 6 particles run parallel on 4 cores) and acceleration constants $c_1 = c_2 = 1.2$. In addition, the quality of

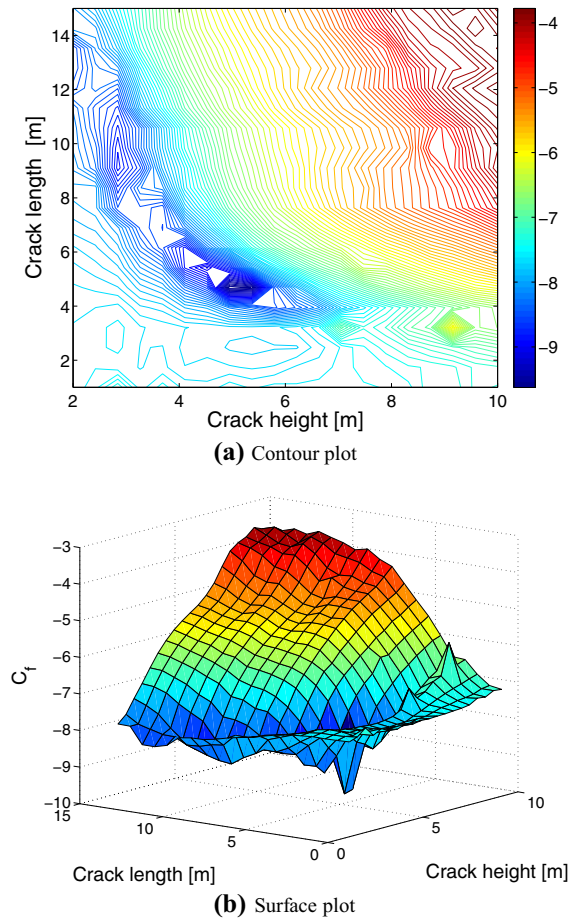


Fig. 9 Log of objective function value in time domain (17 sensors). The trough-like regions seen in (a, b) leads to premature convergence and non-unique parameter values

convergence was influenced by the size of the search area and also the number of excitation points (with positions in Fig. 2b). In the case where a single excitation point is used, 101 function evaluations were required and the minimization error was 1.85×10^{-4} . More over the multiple excitation case required 52 function evaluations to arrive at a convergence with minimization error of 8.4×10^{-6} . It should be noted that for multiple excitation points, the computational time for 1 evaluation is much longer than when only single excitation point is considered. Data used for the evaluation did not consider the effect of noise in measurement. From the obtained results in Fig. 12 using excitation points $E1, E2$ and $E3$ enabled an exact location of the horizontal crack and also a close approximation for the inclined crack although more computation effort was required. This is because better

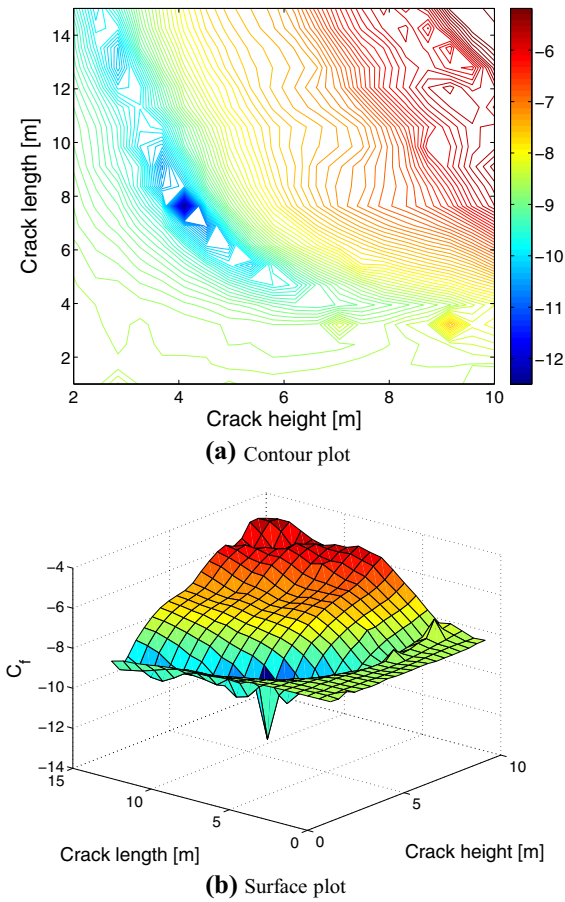


Fig. 10 Log of objective function value in frequency domain (17 sensors). Less trough-like regions in (a, b), most important is a clearly defined global minima

quality response is obtained from excitations closest to (and above) the crack. Thus, using excitation sources are at different sensitive positions within the dam increases the probability of localizing the crack.

To avoid ‘inverse-crime’ (Colton and Kress 2012) and further test the robustness of our method, the effect of noise on the quality of the identified crack parameters is investigated. This is done by corrupting the synthetically generated experimental data used for the inverse analysis. Since the inverse analysis is carried out in the frequency domain, the noise is added to the data in considering two different scenarios. Firstly the time domain measurements are corrupted before transformation to the frequency domain as obtained in Eq. 37. This has the effect of smoothening some of the noise as seen in Fig. 13a. The second scenario deals with noise addition to the frequency

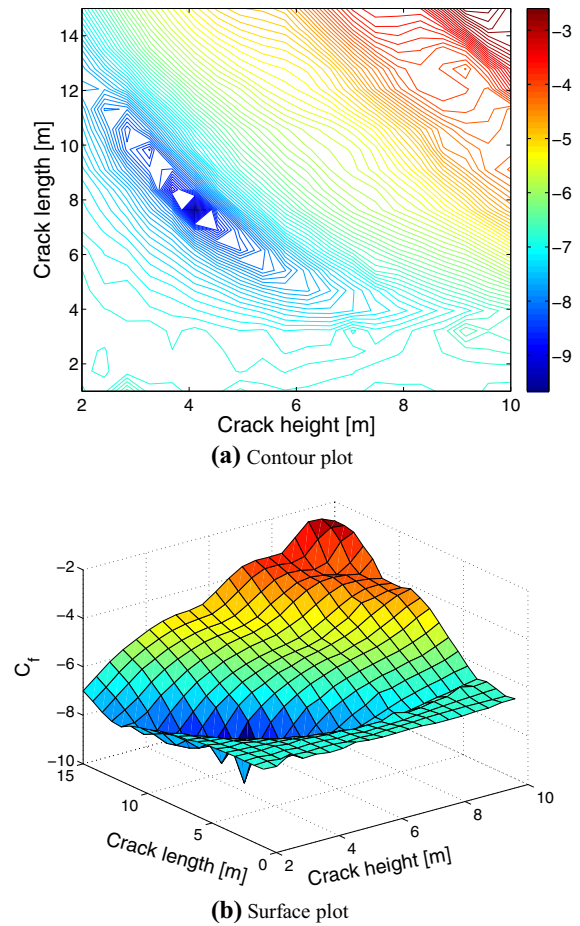


Fig. 11 Multiple excitation objective function value in frequency domain (log). a, b Smoother with fewer local minima as compared to the previous figures. This lowers the probability of converging to a local minima

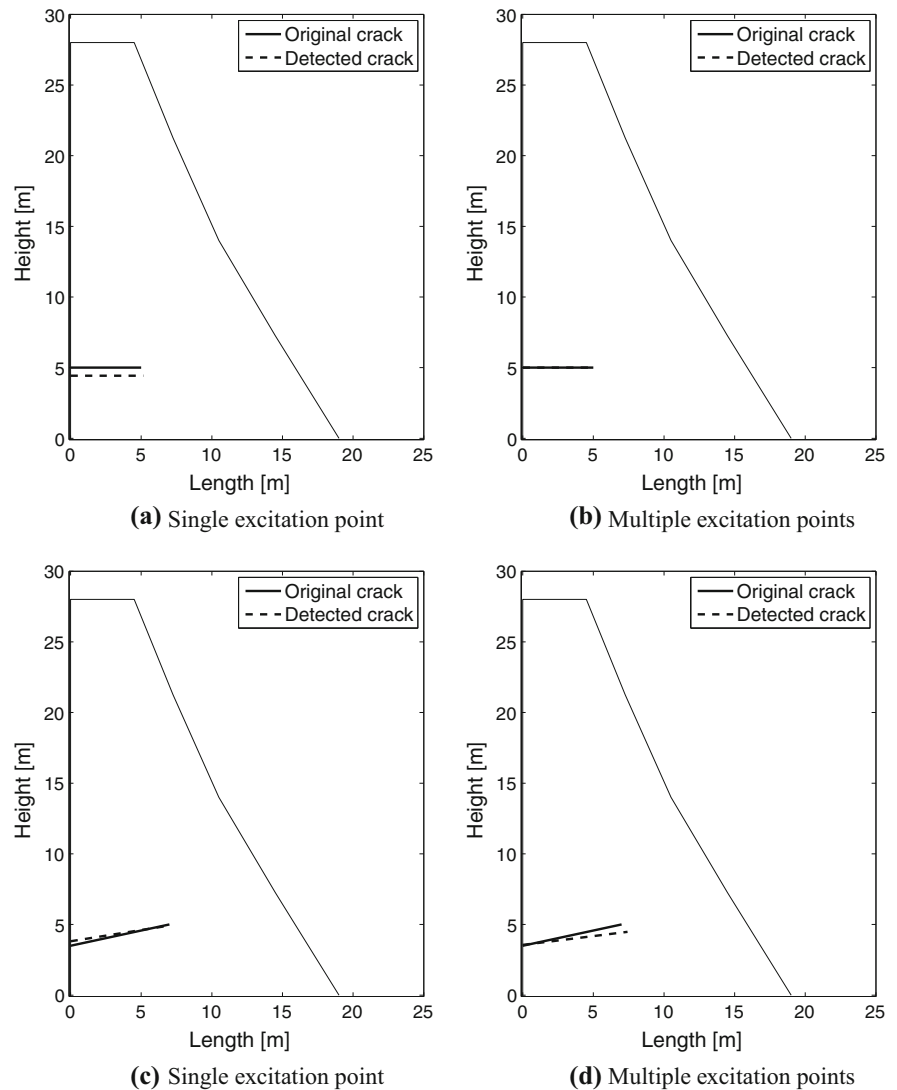
response measurements in Eq. 38, the effect of this on the dam response can be observed in Fig. 13b. The data is corrupted using random normal distributed noise of 1, 5, 10, 20, 25, and 50% before carrying out the inverse analysis.

$$\ddot{U}_{(j,t_i)}^{cor} = \ddot{U}_{(j,t_i)}^{exp} (1 + \mathcal{D} \mathbb{N}); \quad \ddot{U}_{(j,\omega)}^{cor} = \mathcal{F} \left(\ddot{U}_{(j,t_i)}^{cor} \right) \tag{37}$$

$$\ddot{U}_{(j,\omega)}^{cor} = \ddot{U}_{(j,\omega)}^{exp} (1 + \mathcal{D} \mathbb{N}); \tag{38}$$

where $\ddot{U}_{(j,t_i)}^{cor}$ is the corrupted sensor measurement in the time domain, $\ddot{U}_{(j,\omega)}^{cor}$ is the corrupted measurement

Fig. 12 Crack identification using single and multiple excitation points for both horizontal and inclined cracks without noise. **a, b** Compares the quality of fit from applying single or multiple excitation for horizontal crack identification, whereas **(c, d)** makes a comparison for inclined crack identification

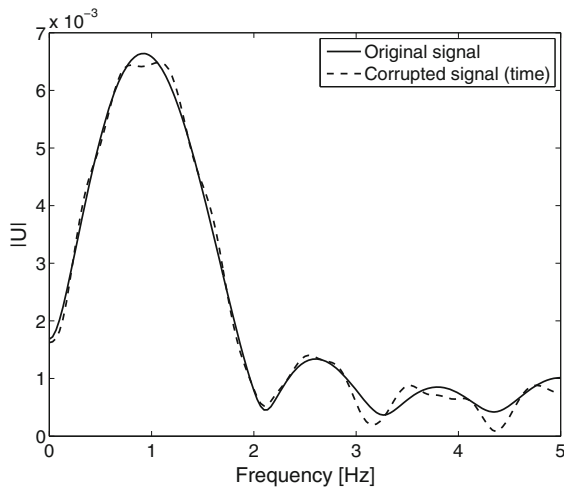


in the frequency domain, ϑ is the percentage of noise added to the signal and \mathbb{N} is the applied noise vector.

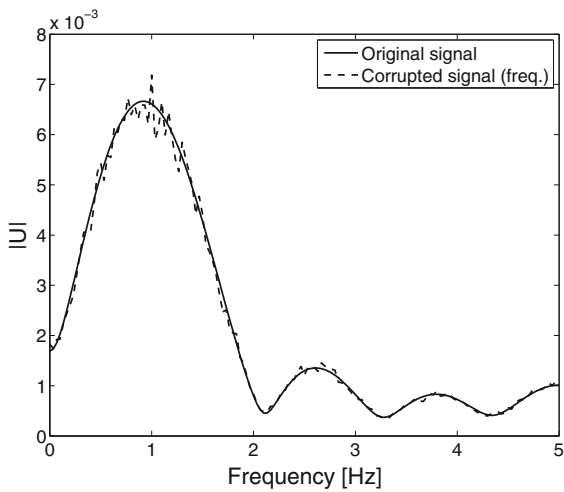
The effect of applying different percentages of noise to both time signal before frequency transformation and to the frequency response of the dam is investigated. The identified crack parameters and final error after the inverse analysis (i.e. with 30 evaluations) for each level of noise considering both the application of a single excitation source and multiple excitation sources are obtained in Table 3 and Fig. 14.

Although investigation into the application of single and multiple excitation sources (as stated in

previous paragraphs) favors the robustness associated with multiple sources, however Table 3 and Fig. 14 shows otherwise. The crack orientation using a single source excitation deviates from the real crack for high noise values. For multiple source excitation, this effect is observed earlier coupled with a higher minimization error as would be expected when comparing Eqs. 35 with (36). The underlying reasons behind this behavior results from the fact that with multiple sources the search space is unrestricted (unlike for single source) and also the noise/error in measurements accumulates for each source. A close observation at Fig. 14 shows a linear increase in the error between both plots as the percentage of noise increases. In practice since the



(a) Time corrupted data response



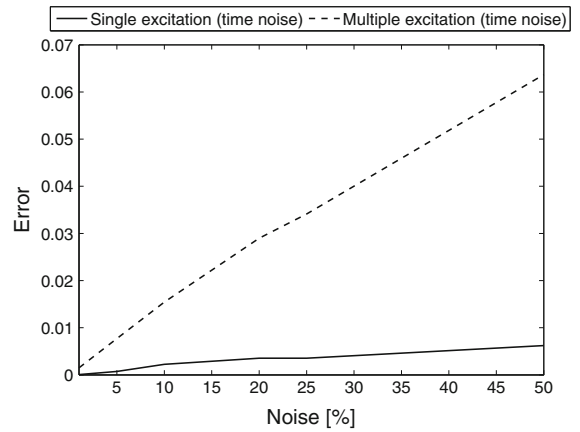
(b) Frequency corrupted data response

Fig. 13 Comparison between original and corrupted dam response. **a** The distortion of the dam response by noise addition in the time domain. **b** Response distortion due to noise addition in the frequency domain

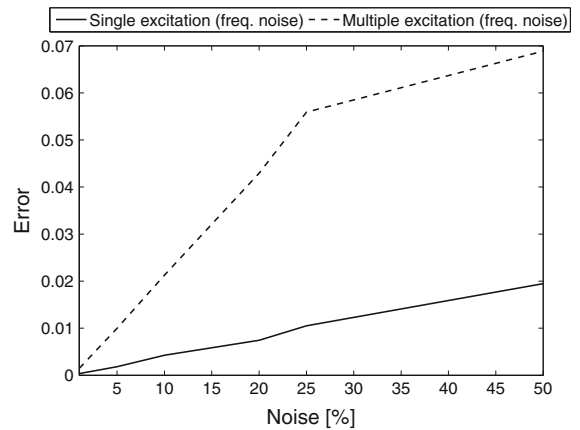
exact distribution of error in measurement is uncertain, it is recommended to first use the multiple excitation method to localize the crack or region where the damage exists, after which data from the excitation source closest to the crack (this constitutes a restricted search space) location can be used to narrow down the crack location and fine tune the results. Thus the following procedures can be readily applied especially when no prior knowledge on the damage region exists

Table 3 Identified crack coordinates for different noise levels

Noise (%)	Crack parameters (x_1, x_2, y_1, y_2)							
	Single excitation				Multiple excitation			
–	0	7	3.5	5	0	7	3.5	5
1	0	6.5	3.7	4.8	0	5.5	6	6
5	0	6.8	3.4	5.5	0	8	6	3.7
10	0	4.2	1.2	5.3	0	5.8	5.2	1.2
20	0	6.9	1	3.5	0	7.9	6	5.8
25	0	7.9	6	5.7	0	7	5.6	6



(a) Time domain noise



(b) Frequency domain noise

Fig. 14 Comparison between quality of fit for single and multiple excitation considering different noise levels. **a** Noise is added to time domain response before transformation and in **(b)** noise is added to the recorded frequency response

1. Carry out multiple excitation of the dam.
2. Obtain all necessary sensor data and measurements.
3. Initiate the inverse analysis using the multiple sources. This is capable of localizing the damage zone.
4. Using output from (3) to restrict search, run inverse analysis using single source and the sensors in this region or the closest to the localized region in (3).
5. Results obtained have a higher probability of convergence to the original crack location.

5 Conclusion

In order to reduce the risk of a catastrophe resulting from dam failure, proper maintenance and monitoring is required. Although synthetic data was used in this work, the damage identification method presented here shows optimism in the location of cracks considering the influence of pore water pressures on the dam. The damping effect of the water in the reservoir on the response amplitude was also simulated by the model. The presence of structural damage can also be detected earlier first from the comparison of frequency response between measurements taken at different time periods where a phase shift of the fundamental frequencies in the measurements triggers an inverse analysis procedure to localize the damage. The frequency domain response showed more sensitivity to structural damage as compared to time domain response.

The application of multiple excitation sources apart from the fact that it requires more computational costs is capable of localizing the damage region irrespective of the search space size. More so, owing to the uncertainty in field measurements, absence of a priori information and the sensitivity of the single excitation method to the search space, a combination of the both the multiple excitation case and the single excitation case is recommended for crack identification. Thus, the proposed method in combination with other structural health monitoring strategies can go a long way in improving current dam monitoring practices and also act as an early warning system for both old and newly constructed dams.

Acknowledgements The authors gratefully acknowledge the financial support of the Thüringer Graduiertenförderung and the German Research Foundation (DFG) under the Grant LA - 2869/4-1.

References

- Ahmadi, M., Izadinia, M., Bachmann, H.: Discrete crack joint model for nonlinear dynamic analysis of concrete arch dam. *Comput. Struct.* **79**(4), 403–420 (2001)
- Alalade, M., Kafle, B., Wuttke, F., Lahmer, T.: Calibration of cyclic constitutive models for soils by oscillatory functions. In: Gürlebeck, K., Lahmer, T. (eds.) *Digital Proceedings, International Conference on the Applications of Computer Science and Mathematics in Architecture and Civil Engineering: July 20–22 2015*. Bauhaus-University Weimar, Weimar (2015)
- Alalade, M.E., Kafle, B., Wuttke, F., Lahmer, T.: Inverse analysis of cyclic constitutive models for unsaturated soil under consideration of oscillating functions. In: *E3S Web of Conferences*, vol. 9, p. 08012. EDP Sciences (2016)
- Ayari, M., Saouma, V.: A fracture mechanics based seismic analysis of concrete gravity dams using discrete cracks. *Eng. Fract. Mech.* **35**(1–3), 587–598 (1990)
- Belytschko, T., Black, T.: Elastic crack growth in finite elements with minimal remeshing. *Int. J. Numer. Methods Eng.* **45**(5), 601–620 (1999)
- Belytschko, T., Gracie, R., Ventura, G.: A review of extended/generalized finite element methods for material modeling. *Model. Simul. Mater. Sci. Eng.* **17**(4), 043,001 (2009)
- Bhattacharjee, S., Lger, P.: Application of NLFM models to predict cracking in concrete gravity dams. *J. Struct. Eng. US* **120**(4), 1255–1271 (1994)
- Béchet, E., Scherzer, M., Kuna, M.: Application of the X-FEM to the fracture of piezoelectric materials. *Int. J. Numer. Methods Eng.* **77**(11), 1535–1565 (2009)
- Chahine, E., Laborde, P., Pommier, J., Renard, Y., Salaün, M.: Study of some optimal XFEM type methods. In: Leitao, V.M.A., Alves, C.J.S., Armando Duarte, C. (eds.) *Advances in Meshfree Techniques*, pp. 27–38. Springer (2007)
- Chatzi, E.N., Hiriyyur, B., Waisman, H., Smyth, A.W.: Experimental application and enhancement of the XFEM–GA algorithm for the detection of flaws in structures. *Comput. Struct.* **89**(7), 556–570 (2011)
- Chopra, A.K.: *Dynamics of Structures*, vol. 3. Prentice Hall, Upper Saddle River (1995)
- Chowdhury, I., Dasgupta, S.P.: Computation of Rayleigh damping coefficients for large systems. *Electron. J. Geotech. Eng.* **8**, 1–11 (2003)
- Colton, D., Kress, R.: *Inverse Acoustic and Electromagnetic Scattering Theory*, vol. 93. Springer, New York (2012)
- Coussy, O.: *Mechanics of Porous Continua*. Wiley, New York (1995)
- De Borst, R., Réthoré, J., Abellan, M.A.: A numerical approach for arbitrary cracks in a fluid-saturated medium. *Arch. Appl. Mech.* **75**(10–12), 595–606 (2006)
- Eberhart, R.C., Kennedy, J.: A new optimizer using particle swarm theory. In: *Proceedings of the Sixth International*

- Symposium on Micro Machine and Human Science, vol. 1, pp. 39–43. New York (1995)
- Feltrin, G., Bachmann, H., Wepf, D.: Seismic Cracking of Concrete Gravity Dams. Birkhäuser, Basel (1991)
- Ghaemian, M., Ghobarah, A.: Nonlinear seismic response of concrete gravity dams with dam-reservoir interaction. *Eng. Struct.* **21**(4), 306–315 (1999)
- Guanglun, W., Pekau, O., Chuhan, Z., Shaomin, W.: Seismic fracture analysis of concrete gravity dams based on nonlinear fracture mechanics. *Eng. Fract. Mech.* **65**(1), 67–87 (2000)
- Ingraffea, A.R., Saouma, V.: Numerical modeling of discrete crack propagation in reinforced and plain concrete. In: *Fracture Mechanics of Concrete: Structural Application and Numerical Calculation*, pp. 171–225. Springer, Netherlands (1985)
- Jing, L., Ma, Y., Fang, Z.: Modeling of fluid flow and solid deformation for fractured rocks with discontinuous deformation analysis (DDA) method. *Int. J. Rock Mech. Min. Sci.* **38**(3), 343–355 (2001)
- Jung, J., Jeong, C., Taciroglu, E.: Identification of a scatterer embedded in elastic heterogeneous media using dynamic XFEM. *Comput. Methods Appl. Mech. Eng.* **259**, 50–63 (2013)
- Khoei, A.R.: *Extended Finite Element Method: Theory and Applications*. Wiley, New York (2014)
- Khoei, A., Vahab, M., Haghighat, E., Moallemi, S.: A mesh-independent finite element formulation for modeling crack growth in saturated porous media based on an enriched-FEM technique. *Int. J. Fract.* **188**(1), 79–108 (2014)
- Lahmer, T.: Crack identification in hydro-mechanical systems with applications to gravity water dams. *Inverse Probl. Sci. Eng.* **18**(8), 1083–1101 (2010)
- Lahmer, T., Rafajlowicz, E.: On the optimality of harmonic excitation as input signals for the characterization of parameters in coupled piezoelectric and poroelastic problems. *Mech. Syst. Signal Process.* **90**, 399–418 (2017)
- Lee, J., Fenves, G.L.: Plastic-damage model for cyclic loading of concrete structures. *J. Eng. Mech.* **124**(8), 892–900 (1998)
- Lewis, R.W., Schrefler, B.A.: *The Finite Element Method in the Static and Dynamic Deformation and Consolidation of Porous Media*. Wiley, New York (1998)
- Lger, P., Leclerc, M.: Evaluation of earthquake ground motions to predict cracking response of gravity dams. *Eng. Struct.* **18**(3), 227–239 (1996)
- Minagawa, K., Suga, K., Kikuchi, M., Aoki, S.: An efficient inverse analysis considering observation error to detect corrosion in concrete structures containing multilayered rebar. *Int. J. Mech. Mater. Des.* **8**(1), 81–87 (2012)
- Nanthakumar, S., Lahmer, T., Rabczuk, T.: Detection of multiple flaws in piezoelectric structures using XFEM and level sets. *Comput. Methods Appl. Mech. Eng.* **275**, 98–112 (2014)
- Nanthakumar, S., Lahmer, T., Zhuang, X., Zi, G., Rabczuk, T.: Detection of material interfaces using a regularized level set method in piezoelectric structures. *Inverse Probl. Sci. Eng.* **24**(1), 153–176 (2016)
- Nelder, J.A., Mead, R.: A simplex method for function minimisation. *Comput. J.* **7**, 308–313 (1965)
- Nguyen-Tuan, L., Datcheva, M., Schanz, T.: Numerical simulation and back analysis of coupled thermo-hydro-mechanical behavior of Sand–Bentonite mixture. In: *18th International Conference on the Application of Computer Science and Mathematics in Architecture and Civil Engineering* (2009)
- Nguyen-Tuan, L., Lahmer, T., Datcheva, M., Stoimenova, E., Schanz, T.: A novel parameter identification approach for buffer elements involving complex coupled thermo-hydro-mechanical analyses. *Comput. Geotech.* **76**, 23–32 (2016)
- Nguyen-Vinh, H., Bakar, I., Msekh, M., Song, J.H., Muthu, J., Zi, G., Le, P., Bordas, S.P.A., Simpson, R., Natarajan, S., et al.: Extended finite element method for dynamic fracture of piezo-electric materials. *Eng. Fract. Mech.* **92**, 19–31 (2012)
- Osher, S., Sethian, J.A.: Fronts propagating with curvature-dependent speed: algorithms based on Hamilton–Jacobi formulations. *J. Comput. Phys.* **79**(1), 12–49 (1988)
- Pan, J., Zhang, C., Xu, Y., Jin, F.: A comparative study of the different procedures for seismic cracking analysis of concrete dams. *Soil Dyn. Earthq. Eng.* **31**(11), 1594–1606 (2011)
- R éthoré, J., De Borst, R., Abellan, M.A.: A discrete model for the dynamic propagation of shear bands in a fluid-saturated medium. *Int. J. Numer. Anal. Methods Geomech.* **31**(2), 347–370 (2007)
- Rabczuk, T., Belytschko, T.: Cracking particles: a simplified meshfree method for arbitrary evolving cracks. *Int. J. Numer. Methods Eng.* **61**(13), 2316–2343 (2004)
- Rabczuk, T., Zi, G., Bordas, S., Nguyen-Xuan, H.: A simple and robust three-dimensional cracking-particle method without enrichment. *Comput. Methods Appl. Mech. Eng.* **199**(37), 2437–2455 (2010)
- Rabinovich, D., Givoli, D., Vigdergauz, S.: XFEM-based crack detection scheme using a genetic algorithm. *Int. J. Numer. Methods Eng.* **71**(9), 1051–1080 (2007)
- Rabinovich, D., Givoli, D., Vigdergauz, S.: Crack identification by arrival time using XFEM and a genetic algorithm. *Int. J. Numer. Methods Eng.* **77**(3), 337–359 (2009)
- Segura, J.M., Carol, I.: Coupled HM analysis using zero-thickness interface elements with double nodes. Part I: theoretical model. *Int. J. Numer. Anal. Methods Geomech.* **32**(18), 2083–2101 (2008)
- Singh, I.V., Mishra, B.K., Bhattacharya, S.: Xfem simulation of cracks, holes and inclusions in functionally graded materials. *Int. J. Mech. Mater. Des.* **7**(3), 199 (2011)
- Sun, H., Waisman, H., Betti, R.: A multiscale flaw detection algorithm based on XFEM. *Int. J. Numer. Methods Eng.* **100**(7), 477–503 (2014)
- Sun, H., Waisman, H., Betti, R.: A sweeping window method for detection of flaws using an explicit dynamic XFEM and absorbing boundary layers. *Int. J. Numer. Methods Eng.* **105**, 1014–1040 (2015)
- Waisman, H., Chatzi, E., Smyth, A.W.: Detection and quantification of flaws in structures by the extended finite element method and genetic algorithms. *Int. J. Numer. Methods Eng.* **82**(3), 303–328 (2010)
- Wang, G., Wang, Y., Lu, W., Zhou, C., Chen, M., Yan, P.: XFEM based seismic potential failure mode analysis of concrete gravity dam–water–foundation systems through

- incremental dynamic analysis. *Eng. Struct.* **98**, 81–94 (2015)
- Zhang, S., Wang, G., Yu, X.: Seismic cracking analysis of concrete gravity dams with initial cracks using the extended finite element method. *Eng. Struct.* **56**, 528–543 (2013)
- Zhang, C., Wang, C., Lahmer, T., He, P., Rabczuk, T.: A dynamic XFEM formulation for crack identification. *Int. J. Mech. Mater. Des.* **12**(4), 427–448 (2015)
- Zheng, D., Huo, Z., Li, B.: Arch-dam crack deformation monitoring hybrid model based on XFEM. *Sci. China Technol. Sci.* **54**(10), 2611–2617 (2011)
- Zienkiewicz, O., Shiomi, T.: Dynamic behaviour of saturated porous media: the generalized biot formulation and its numerical solution. *Int. J. Numer. Anal. Methods Geomech.* **8**(1), 71–96 (1984)
- Zienkiewicz, O., Chan, A., Pastor, M., Paul, D., Shiomi, T.: Static and dynamic behaviour of soils: a rational approach to quantitative solutions. I. Fully saturated problems. In: *Proceedings of the Royal Society of London A: Mathematical, Physical and Engineering Sciences*, vol. 429, pp. 285–309. The Royal Society (1990)
- Zlotnik, S., Díez, P., Fernández, M., Vergés, J.: Numerical modelling of tectonic plates subduction using X-FEM. *Comput. Methods Appl. Mech. Eng.* **196**(41), 4283–4293 (2007)